Quantum approximation to regular and chaotic classical motion: An electron in two periodic potentials

J. C. Kimball, Vijay A. Singh,* and Mark D'Souza
Physics Department, State University of New York at Albany, Albany, New York 12222
(Received 19 November 1991)

An electron in a periodic crystal potential, which is subjected to an additional periodic pulsed potential, is an example of a system which can be modeled by the kicked Harper model. The relative simplicity of this model facilitates a comparison of its quantum and classical dynamics. The model has a clearly defined semiclassical limit in which wave packets follow the classical motion. A power series in $\hbar$ yields systematic quantum corrections to the semiclassical limit. Numerical iterations of the quantum equations agree with the $\hbar$ expansion (for a limited time), provided the corresponding classical motion is not chaotic. For chaotic motion, the agreement between classical and quantum motion disappears very quickly. The quantum solutions also show (i) precursors to classical chaos, (ii) a time-dependent analog of wave-function scarring, and (iii) quantum echoes arising from quantized phase-space orbits.

PACS number(s): 05.45.+b, 03.65.Sq, 73.20.Dx

I. INTRODUCTION

"Chaos" is often regarded as a purely classical effect [1]. But classical physics is the large-quantum-number limit of quantum mechanics. When quantum numbers approach infinity, wave packets follow classical trajectories. The interplay of classical chaos with quantum effects occurs for large, but finite, quantum numbers. Specific models which have chaotic classical analogs show surprising properties [2–4]. These include suppressed diffusion [5,6], counterintuitive tunneling [7], "scarred" wave functions [8], and anomalous energy-level statistics [9].

There are several reasons to choose the kicked Harper model for a study of the relation between classical chaos and quantum mechanics. First, the model is related to real physical systems. For example, it has been used as a model of an electron in perpendicular magnetic and electric fields [10]. The magnetic field is time independent, but the electric field is periodically pulsed. The kicked Harper model can also be used to describe an electron hopping through a crystal which is subjected to a pulsed electric field, and we will use this alternate physical picture to motivate our quantum version of the model. Second, the model is relatively simple because it can be constructed with special symmetries [11,12], and the quantum version of the model is restricted to a finite-dimensional state space. This enables us to derive results using a relatively simple formalism. Finally, both the classical [13–15] and quantum [16–18] forms of this model have been carefully studied.

Our investigation of the kicked Harper model is both formal and numerical. The formal results are based on an expansion in powers of $\hbar$ (actually, an inverse-quantum-number expansion). The lowest-order terms in this expansion give the semiclassical limit. In this limit, the centroid of a localized wave packet (called $\langle\theta\rangle$) follows the classical motion, and the spread of the wave packet (called $\langle\Delta\theta^2\rangle$) is determined by the stability of the classical motion. Higher-order quantum corrections to the semiclassical motion are especially large when the classical motion is chaotic.

Our numerical results are more than a check on these formal results. They reveal effects not captured by the leading terms in the $\hbar$ expansion. These include the time-dependent analog of wave-function scarring, and "quantum echoes" associated with semiclassical quantization of the phase-space orbits.

II. KICKED HARPER MODEL

The kicked Harper model can be used to describe an electron in a one-dimensional crystal which is subjected to a periodically pulsed sinusoidal potential. In a simple tight-binding approximation, the crystal environment yields kinetic energies proportional to $\cos(pd)$, where p is the crystal-momentum wave vector, and d is the lattice constant. The pulsed potential energy is assumed to be proportional to $\cos(2\pi x/\lambda)$, where x is the position and λ is the wavelength of the potential. The sum of the kinetic and potential energies is periodic in both the momentum and position coordinates, so it is convenient to represent the system in terms of angles θ and ϕ which are proportional to the position and momentum of the particle:

$$\phi=pd \ , \quad \theta=\frac{2\pi x}{\lambda} \ . \tag{1}$$

A. Classical model

The classical kicked Harper model is described by a Hamiltonian which is the sum of the kinetic and potential energies of the form discussed above:

$$H_{\rm cl}=-\frac{g}{\tau}\left[\cos(\phi)+\tau\sum_l \delta(t-l\tau)\cos(\theta)\right] . \tag{2}$$

 ©1992 The American Physical Society

Here we have used the dimensionless variables θ and ϕ instead of the physical momentum and position coordinates. The sum of δ functions in Eq. (2) causes the pulsing of the potential-energy term. For simplicity and symmetry, the width of the energy band and the strength of the time-averaged potential energy are characterized by the same coupling constant, g. Hamilton's equations

$$\frac{d\theta}{dt}=\frac{\partial H}{\partial\phi}\ ,\quad \frac{d\phi}{dt}=-\frac{\partial H}{d\theta} \tag{3}$$

give a description of the classical motion in terms of the recursion relations

$$\phi_{n+1}=\phi_n-g\sin(\theta_n)\ ,\quad \theta_{n+1}=\theta_n+g\sin(\phi_{n+1})\ , \tag{4a}$$

where θ_n and ϕ_n are the coordinates just before the nth pulse. These coupled equations [Eq. (4a)] are the essence of the classical kicked Harper model. They lead to complex "webs" of stochastic behavior when the parameter g is sufficiently large [13,15].

B. Quantum model

The quantum version of the kicked Harper model is obtained by returning to the physical example of a particle moving on a lattice. The degree of "quantumness" of the model is determined by a parameter N, which is the ratio of the wavelength of the periodic potential, λ, to the lattice constant d. Large N corresponds to the classical limit, while the small-N model is clearly quantum mechanical. For simplicity, we take N to be an integer, so the Hamiltonian has a period of N lattice sites. We apply periodic boundary conditions to this N-site system, so the model describes a particle hopping along an N-site ring which is subjected to a periodically pulsed sinusoidal potential. Wave functions are linear combinations of orbitals $|n\rangle$ localized at lattice sites, with $-N/2<n\le N/2$, and the quantum Hamiltonian is determined by its action on these localized states:

$$H|n\rangle=-\frac{g}{\tau}\left[\frac{1}{2}(|n+1\rangle+|n-1\rangle)+\left[\tau\sum_l\delta(t-l\tau)\right]\cos\left[\frac{2\pi}{N}n\right]|n\rangle\right]\ . \tag{5a}$$

The similarity of this Hamiltonian to the classical Harper model can be seen by examining the potential- and kinetic-energy terms separately. The potential of the above Hamiltonian gives the classical potential energy when operating on the localized state, $|n\rangle$, provided one associates the angle θ with the lattice sites through

$$\theta\approx\frac{2\pi}{N}n\ . \tag{6a}$$

The correspondence with the classical kinetic energy is obtained through a Fourier transform from the localized states to Bloch states, defined for integers $-N/2<k\le N/2$ as

$$|k\}=\frac{1}{\sqrt{N}}\sum_n\exp\left[i\frac{2\pi}{N}kn\right]|n\rangle\ . \tag{7}$$

Substituting the Bloch states $|k\}$ into the Hamiltonian gives

$$H|k\}=-\frac{g}{\tau}\left[\cos\left[\frac{2\pi}{N}k\right]|k\}+\frac{1}{2}\left[\tau\sum_l\delta(t-l\tau)\right]\times(|k+1\}+|k-1\})\right]\ . \tag{5b}$$

Thus the first term of the quantum Hamiltonian operating on the Bloch states gives the kinetic energy of the classical Hamiltonian [Eq. (2)] through the correspondence

$$\phi\approx\frac{2\pi}{N}k\ . \tag{6b}$$

Of course the difference between the classical and quantum versions of this model lies in the impossibility of finding simultaneous quantum eigenstates of both the kinetic- and potential-energy terms. However, in the large-N limit, Gaussian wave packets come close to having well-defined kinetic and potential energies. A Gaussian wave packet characterized by a "width parameter" α centered at site n_0 with a mean wave vector k_0 is

$$|\alpha,n_0,k_0\rangle\equiv\mathcal{N}\sum_n\exp\left[\frac{2\pi}{N}[ik_0(n-n_0)-\alpha(n-n_0)^2/2]\right]|n\rangle\ , \tag{8a}$$

where $\mathcal{N}=[2\,\mathrm{Re}(\alpha)/N]^{1/4}$.

The large-N limit is analogous to a vanishing Planck's constant. The relation between N and $\hbar$ can be obtained through an uncertainty principle. The width of the Gaussian wave packet is

$$\langle\alpha,n_0,k_0|(n-n_0)^2|\alpha,n_0,k_0\rangle=\frac{N}{4\pi\,\mathrm{Re}\alpha}\ . \tag{9a}$$

Scaling n by $2\pi/N$ to express this width in terms of the angle θ gives

$$\langle\Delta\theta^2\rangle=\frac{\pi}{N\,\mathrm{Re}\alpha}\ . \tag{9b}$$

Similarly, transforming to the Bloch states gives the momentum-space width of the wave packet.

$$\langle\Delta\phi^2\rangle=\frac{\pi}{N\mathrm{Re}(1/\alpha)}\ . \tag{9c}$$

Taking the product of these widths yields a Heisenberg-like uncertainty principle.

$$(\langle\Delta\theta^2\rangle\langle\Delta\phi^2\rangle)^{1/2}\ge\frac{\pi}{N} \tag{10}$$

with equality obtained only when α is real. One traditionally expects the minimum uncertainty to be $\hbar/2$, so we define an effective Planck's constant as

$$\hbar=\frac{2\pi}{N} . \tag{11}$$

This $\hbar$ is dimensionless because it expresses the uncertainty in the dimensionless position and momentum angles (θ and ϕ).

Even when α is not real, Gaussian wave packets are maximally localized. The phase-space distribution (Wigner function) associated with these Gaussian wave packets is largely confined to an ellipse with area $\approx\pi\hbar$ which is centered about the mean position (θ_0,ϕ_0). When α is real, the major and minor axes of this ellipse are along the θ and ϕ directions. A complex α means the ellipse is not aligned with the θ and ϕ axes. This leads to a larger uncertainty, $(\langle\Delta\theta^2\rangle\langle\Delta\phi^2\rangle)^{1/2}$, even though the occupied area of phase space remains $\approx\pi\hbar$.

III. QUANTUM TIME EVOLUTION

The correspondence between the classical and quantum motion of this model is obtained using wave packets. The action of the quantum time-evolution operator shows that the wave-packet centroid follows the classical motion for times which become large as $\hbar$ vanishes. Differences between the classical and quantum motion are seen in the broadening and distortion of the wave packets, and this leads to a difference between the position of the wave-packet centroid and the classical trajectory.

A. Wave packets

In order to describe the distortion of wave packets, it is not sufficient to consider only Gaussian ones. The wave-packet space must be expanded to include Gaussian functions multiplied by powers, defined as

$$|\alpha,n,k,j\rangle\equiv\mathcal{N}\frac{\hbar^{j/2}}{j!}\sum_m\exp[i\hbar k(m-n)-\alpha\hbar(m-n)^2/2]\times(m-n)^j|m\rangle , \tag{8b}$$

where $\mathcal{N}$ is defined as before, and the case $j=0$ corresponds to the ordinary Gaussian wave packets of Eq. (8a). A related set of wave packets, which is defined in terms of the Bloch-basis set, is

$$|\alpha,n,k,j\}\equiv\frac{\mathcal{N}}{\sqrt{\alpha}}\frac{\hbar^{j/2}}{j!}\sum_p\exp[-i\hbar pn-\hbar(p-k)^2/(2\alpha)]\times(p-k)^j|p\} . \tag{8c}$$

When the indices (α,n,k) are clear, we use the shorthand notation $|\alpha,n,k,j\rangle=|j\rangle$, and $|\alpha,n,k,j\}=|j\}$.

The localized-basis and Bloch-basis wave packets are simply related. In particular, Fourier transformation of the localized $j=0$ states gives

$$|0\rangle=|0\} . \tag{12a}$$

Differentiating $|0\rangle$ with respect to k gives

$$|j\rangle=\frac{(-i)^j}{\hbar^{j/2}j!}\frac{\partial^j}{\partial k^j}|0\rangle . \tag{13}$$

Replacing $|0\rangle$ by $|0\}$, and carrying out the differentiation gives

$$|j\rangle=\left[\frac{-i}{\alpha}\right]^j\left[|j\}-\frac{\alpha}{2}|j-2\}+\frac{\alpha^2}{2(4)}|j-4\}-\frac{\alpha^3}{2(4)6}|j-6\}+\cdots\right] , \tag{12b}$$

where the series terminates with state $|1\}$ or state $|0\}$. The inverse transformation (from $|j\}$ to $|j\rangle$) is obtained by multiplying both types of states by $\exp(-i\hbar kn)$. Then it is apparent that the relations are inverted by replacing i by $-i$ and α by $1/\alpha$.

B. Time-evolution operator

The time evolution is obtained from the operator [19,20]

$$U(t',t)=T\left[\exp\left[-\frac{i}{\hbar}\int_t^{t'}H(\tilde{t})d\tilde{t}\right]\right] , \tag{14}$$

where T denotes time ordering. Because the potential energy is pulsed, the time evolution for one period τ, starting with a pulse of the potential and ending just before the next pulse, is $U(\tau^-,0^-)=U_KU_V$, where U_V and U_K represent the time evolution generated by the potential- and kinetic-energy terms in $H(t)$. The operator U_V multiplies the localized states $|n\rangle$ by a phase factor.

$$U_V|n\rangle=\exp[i(g/\hbar)\cos(\hbar n)]|n\rangle , \tag{15a}$$

where g is the same parameter which appears in the classical version of this model. Similarly, in the time interval up to the next pulse, the time evolution changes the phases of the Bloch states.

$$U_K|k\}=\exp[i(g/\hbar)\cos(\hbar k)]|k\} . \tag{15b}$$

Just as for the classical case, the potential pulse U_V changes the particle's momentum, and the time evolution of the system up to the next pulse U_K keeps the momentum constant but changes the position.

Recursion relations for the time evolution of this model, to a given order in $\hbar$ are obtained from the time evolution of the generalized wave packets defined in Eqs. (8b) and (8c) above. The action of U_V is obtained by expanding the cosine function [see Eq. (15a)] about the center of the wave packet on which it acts. That is, for U_V operating on $|\alpha_0,n_0,k_0,j\rangle$,

$$(g/\hbar)\cos(\hbar n)\cong(g/\hbar)\cos(\hbar n_0)-g\sin(\hbar n_0)(n-n_0)-g\hbar\cos(\hbar n_0)(n-n_0)^2/2 . \tag{15c}$$

By retaining only these terms in the exponential, one obtains a new wave packet with modified k and α. Higher-order terms in the expansion of the cosine are not left in the exponential, but are expanded in a power series to generate wave packets with differing values of j.

The symmetry of the wave packets and the Hamiltonian means one can repeat essentially the same expansion to obtain the operation of U_K. Of course, in order to ex-

ploit this symmetry, one must transform the wave packet to the Bloch states [see Eq. (7)].

C. Semiclassical approximation

Semiclassical results are obtained if the expansion of the cosines in the time-evolution operators U_V and U_K are terminated at the quadratic term. Then the recursion relations involve only simple ($j=0$) Gaussian wave packets, and

$$U_V|\alpha_0,n_0,k_0,0\rangle \cong e^{i\eta}|\tilde{\alpha},n_0,k_1,0\rangle \ , \tag{16}$$

where the phase η is not important for our derivations. The changes in k and α caused by U_V give the first half of the semiclassical recursion relations. In terms of the angle variables,

$$\tilde{\alpha}=\alpha_0+ig\cos(\theta_0) \ , \quad \phi_1=\phi_0-g\sin(\theta_0) \ . \tag{4b}$$

The second half of the recursion relation comes from the equivalent treatment of U_K.

$$(\alpha_1)^{-1}=(\tilde{\alpha})^{-1}+ig\cos(\phi_1) \ , \quad \theta_1=\theta_0+g\sin(\phi_1) \ . \tag{4c}$$

In this semiclassical approximation, θ and ϕ do not depend on α, and the recursion relations for θ and ϕ are identical to the classical recursion relations [Eq. (4a)]. Furthermore, the *relative* broadening of the wave packets, obtained from the recursion relations for α, is also a semiclassical result which does not depend on $\hbar$. Of course the *absolute* wave packet width vanishes with $\hbar$ because, for example,

$$\langle \Delta\theta^2 \rangle = \frac{\hbar}{2\,\mathrm{Re}\alpha} \ . \tag{9b}$$

IV. STABILITY

There is a close relationship between the stability of the classical motion (described in Sec. IV A below) and the dispersion of the corresponding Gaussian wave packet (described in Sec. IV B). For example, in the semiclassical approximation, stable classical *periodic* orbits imply the existence of nondispersive wave packets. At the other extreme, unstable classical motion corresponds to wave packets which rapidly disperse.

A. Classical stability

The classical recursion relations for ϕ and θ can be written

$$\begin{bmatrix}\phi_1\\ \theta_1\end{bmatrix}=\begin{bmatrix}\phi_0-g\sin(\theta_0)\\ \theta_0+g\sin[\phi_0-g\sin(\theta_0)]\end{bmatrix} \ . \tag{4d}$$

A more compact notation is useful. Let the two-dimensional vector P correspond to the phase-space position, with the initial position

$$P_0=\begin{bmatrix}\phi_0\\ \theta_0\end{bmatrix} \ . \tag{17}$$

Denote the recursion relation by the function $f(\ )$, so after two iterations,

$$P_2=f(P_1)=f(f(P_0)) \ . \tag{18}$$

The character of the motion generated by these recursion relations ("stable or unstable," "regular or chaotic") is revealed by infinitesimal variation of the initial point P_0. Differentiating $P_1=f(P_0)$ with respect to P_0 gives the matrix equation

$$\begin{bmatrix}\delta\phi_1\\ \delta\theta_1\end{bmatrix}=\begin{bmatrix}1 & -g\cos(\theta_0)\\ g\cos(\phi_1) & 1-[g\cos(\phi_1)][g\cos(\theta_0)]\end{bmatrix} \times\begin{bmatrix}\delta\phi_0\\ \delta\theta_0\end{bmatrix} \ . \tag{19a}$$

Using the more compact notation,

$$\delta P_1=M(P_0)\delta P_0 \ , \tag{19b}$$

where Eq. (19a) defines the "classical stability matrix" $M(P_0)$. Differentiating $P_2=f(f(P_0))$ gives the variation of the second point in terms of the variation of the first point,

$$\delta P_2=M^{(2)}\delta P_0 \ , \tag{20}$$

where

$$M^{(2)}=M(P_1)M(P_0) \ . \tag{21}$$

The generalization to $M^{(s)}$ for s iterations is clear.

B. Quantum stability

The stability of the wave packet is determined by changes in the width parameter α. One generally expects the wave packets to become broader with time as the real part of α shrinks, while its imaginary part grows. This causes both $\mathrm{Re}\alpha$ and $\mathrm{Re}(1/\alpha)$ to become small, so the phase-space "dimensions" of the wave packet become large, even though the total area in phase space remains $\approx\pi\hbar$ in this semiclassical approximation.

The semiclassical time evolution of α is determined by the dispersion relations $\alpha_0\rightarrow\tilde{\alpha}$, and $\tilde{\alpha}\rightarrow\alpha_1$ [see Eqs. (4b) and (4c)]. Combining these gives

$$\alpha_1=\frac{\alpha_0+ig\cos(\theta_0)}{1+[\alpha_0+ig\cos(\theta_0)][ig\cos(\phi_1)]} \ . \tag{22a}$$

This can be written in terms of the classical stability matrix as

$$\alpha_1=\frac{M_{11}\alpha_0-iM_{12}}{iM_{21}\alpha_0+M_{22}} \ , \tag{22b}$$

where M_{ij} are the matrix elements of $M(P_0)$ [see Eq. (19)]. Iterating the above to find α_s in terms of α_0, one finds that the above expression is just the $s=1$ case of the more general equation

$$\alpha_s=\frac{M_{11}^{(s)}\alpha_0-iM_{12}^{(s)}}{iM_{21}^{(s)}\alpha_0+M_{22}^{(s)}} \ . \tag{22c}$$

The close correspondence between wave-packet spreading and the classical stability is clear from the above equation. For example, take α_0 to be unity so the

initial wave packet is optimally localized in the ϕ-θ phase space. Then after s iterations, the θ spread of the wave packet, $\hbar/(2\,\mathrm{Re}\alpha)$, simplifies to

$$\langle \Delta\theta^2 \rangle = \frac{\hbar}{2}[(M_{21}^{(s)})^2+(M_{22}^{(s)})^2] \ . \tag{23}$$

The semiclassical basis of this result is clear. The $(M_{21})^2$ and $(M_{22})^2$ terms are identical to the squares of the classical separation (along θ) of two points which are initially separated by $\sqrt{\hbar/2}$ in the θ and ϕ directions, respectively. An analogous relation holds for $\langle \Delta\phi^2 \rangle$. This confirms our intuitive view that, to lowest order, one can understand wave-packet spreading by simply following a "swarm" of classical trajectories [2], which are initially confined to phase-space ellipse of area $\approx \pi\hbar$. In this semiclassical approximation, time evolution deforms this ellipse, but keeps its area constant. For chaotic motion, the ellipse is stretched until it is very long and thin, and is no longer confined to a small region of phase space. Of course, these results are modified by quantum corrections to the semiclassical limit.

V. QUANTUM CORRECTIONS

Quantum corrections describe changes in the wave-packet shape and position as a power series in $\hbar$, where the semiclassical results are the zero-order terms. The quantum corrections which are linear in $\hbar$ will be described here. The more complicated $\hbar^2$ terms can be obtained from the authors.

The semiclassical results were based on the simple Gaussian wave packets of Eq. (8a). Since quantum corrections describe wave-packet distortion, we must now consider the generalized Gaussian wave-packets defined in Eqs. (8b) and (8c). To order $\hbar$, states of the form

$$|\psi\rangle = |0\rangle + x\sqrt{\hbar}|1\rangle + y\sqrt{\hbar}|3\rangle \tag{24}$$

are closed upon iteration of the time-evolution operator. Here we have used the compact notation $|j\rangle = |\alpha,n,k,j\rangle$. The "distortion parameters" of $|\psi\rangle$, x and y, describe the change in wave-packet shape from a simple Gaussian one.

Recursion relations for x and y are obtained from $U_V|\psi\rangle$ by carrying out the expansion of $\cos(n\hbar)$ to one higher power than was needed for the semiclassical result [Eq. (15c)]. Then converting the $|j\rangle$ states to the $|j\}$ states gives

$$U_V(|0\rangle + x\sqrt{\hbar}|1\rangle + y\sqrt{\hbar}|3\rangle) \cong e^{i\eta}(|\tilde{0}\} + \tilde{x}\sqrt{\hbar}|\tilde{1}\} + \tilde{y}\sqrt{\hbar}|3\}) \ , \tag{25}$$

where

$$\tilde{x} = \frac{ix}{\tilde{\alpha}} - \frac{g\sin\theta}{\tilde{\alpha}^2} + \frac{iy}{\tilde{\alpha}^2} \ , \tag{26a}$$

$$\tilde{y} = -\frac{iy}{\tilde{\alpha}^3} + \frac{g\sin(\theta)}{\tilde{\alpha}^3} \ , \tag{26b}$$

with $\tilde{\alpha}$ given by Eq. (4b). The second half of the recursion relations for x and y is obtained from the analogous expansion of $U_K|\tilde{\psi}\}$. The map $(\tilde{x},\tilde{y}) \rightarrow (x',y')$ is the same as $(x,y) \rightarrow (\tilde{x},\tilde{y})$, except $(i \rightarrow -i)$, $(1/\tilde{\alpha} \rightarrow \alpha')$, and $[\sin(\theta) \rightarrow -\sin(\phi')]$. To this order, α, θ, and ϕ are not affected by x and y.

The first-order quantum corrections to the position and momentum of the wave packet (obtained from $\langle \psi|\theta|\psi \rangle$ and $\langle \psi|\phi|\psi \rangle$) depend only on x and y, and

$$\langle \theta \rangle - \theta_{\mathrm{cl}} \cong \frac{\hbar}{\mathrm{Re}\alpha}\left[\mathrm{Re}x + \frac{\mathrm{Re}y}{4\,\mathrm{Re}\alpha}\right] , \tag{27a}$$

$$\langle \phi \rangle - \phi_{\mathrm{cl}} \cong \frac{\hbar}{\mathrm{Re}(1/\alpha)}\left[\mathrm{Re}\tilde{x} + \frac{\mathrm{Re}\tilde{y}}{4\,\mathrm{Re}(1/\alpha)}\right] , \tag{27b}$$

where θ_{cl} and ϕ_{cl} are obtained from the classical recursion relations. The size of the first quantum correction depends sensitively on the character of the corresponding classical motion. It grows exponentially in time for chaotic motion because it is proportional to the semiclassical wave-packet widths, $\langle \Delta\theta^2 \rangle = \hbar/(2\,\mathrm{Re}\alpha)$ and $\langle \Delta\phi^2 \rangle = \hbar/[2\,\mathrm{Re}(1/\alpha)]$, and these widths grow exponentially for unstable motion. Higher-order quantum corrections to $\langle \theta \rangle$ and $\langle \phi \rangle$ include higher powers of $\hbar/\mathrm{Re}\alpha$ and $\hbar/\mathrm{Re}(1/\alpha)$, so the series quickly diverge for chaotic motion. We have found that the quantum corrections are quantitatively useful only when the motion is stable. Quantum corrections mean the system is not classically deterministic, since knowledge of the initial coordinates ($\langle \theta_0 \rangle$ and $\langle \phi_0 \rangle$) does not predict future values of $\langle \theta \rangle$ or $\langle \phi \rangle$.

VI. NUMERICAL RESULTS

Our numerical calculations have generally confirmed our formal results. For example, we have calculated $\langle \theta \rangle$ by iterating the exact quantum time-evolution equations. If the corresponding classical motion is stable, we find that $\langle \theta \rangle$ follows the classical motion for many iterations, especially for large N. Furthermore, the first-order quantum correction gives a significantly better agreement with the numerical results. On the other hand, the quantum results quickly depart from the corresponding classical motion when that motion is unstable.

Classical motion is either stable or unstable, with essentially no middle ground. However, both our numerical and formal results show that as the quantum system approaches a point of classical instability, it becomes "less stable." The quantum corrections become large after relatively few iterations, and the similarities between classical and quantum motion quickly vanish.

A periodic-orbit example illustrates our results. The sixth-order classical periodic orbit, generated from the initial point $\phi_0 = 0$, and $g\sin(\theta_0) = \theta_0$ is classically stable for $\theta_0 < 2.03$. Values of θ generated by the recursion relations endlessly repeat the sequence $(\theta_0, 0, -\theta_0, -\theta_0, 0, \theta_0)$. For $\theta_0 > 2.03$, the periodic orbit is unstable, and the smallest variations in initial conditions cause deviations from the periodic sequence to increase exponentially.

To compare quantum and classical results for this periodic orbit, we have numerically iterated the quantum dynamics, starting with the Gaussian wave packet

$|\alpha=1,\theta_0,\phi=0,0\rangle$ which is centered at the periodic point. We characterize the ability of the quantum system to follow the classical motion by the iteration number l_c, defined as the first iteration for which the peak in the quantum probability density differs by more than $\theta_0/2$ from the classical result. One would expect l_c to generally increase with N as the quantum system becomes "more classical." The N dependence of l_c for $4 \leq N \leq 150$ is shown in Fig. 1 for $\theta_0=1.85$ and 1.95. Both values of θ_0 correspond to stable classical motion, but the increase of l_c with N is much more apparent for $\theta_0=1.85$ than it is for $\theta_0=1.95$. (Note: for N between 100 and 150, only every tenth point was calculated, and the points were connected by straight lines.)

The apparent failure of the quantum system to follow the classical motion for $\theta_0=1.95$, as suggested by Fig. 1, is not really surprising. We feel it occurs because the Gaussian wave packet spreads into regions of classical instability. Formally, quantum corrections to the classical motion are large when the classical motion is barely stable, so the two systems quickly exhibit differing behavior. For the clsasical limit ($N \to \infty$), both examples in Fig. 1 must follow the regular classical motion. Indeed, we find that the $\theta_0=1.95$ example does become classical, but only when N exceeds ≈ 300.

Our numerical investigations also reveal anomalies of the kicked Harper model which are not apparent in the semiclassical approximation or in the low-order quantum corrections. Two of these anomalies, "scarring" and "quantum echoes," will be described here.

A. Scarring

Scarring has been seen in solutions of the time-independent Schrödinger equation [8]. Typically, the scars appear as especially large values of $\langle\psi|\psi\rangle$ which lie close to periodic orbits. Our model allows us to see time-dependent scarring, where maxima in $\langle\psi|\psi\rangle$ change with time (iteration number), and the position of these maxima corresponds to the position of the corresponding classical motion.

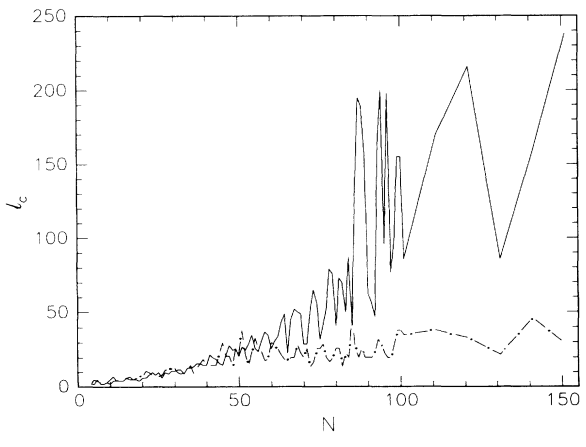

FIG. 1. The number of iterations for which the quantum and classical system agree, l_c, as a function of N. For the full curve $\theta_0=1.85$, and $\theta_0=1.95$ for the dashed curve. Both curves correspond to stable classical motion, but the marginal stability for $\theta_0=1.95$ means reasonable agreement between classical and quantum results is obtained only for $N>300$. (For $100 \leq N \leq 150$, only every tenth point was calculated, and the curves connect these points.)

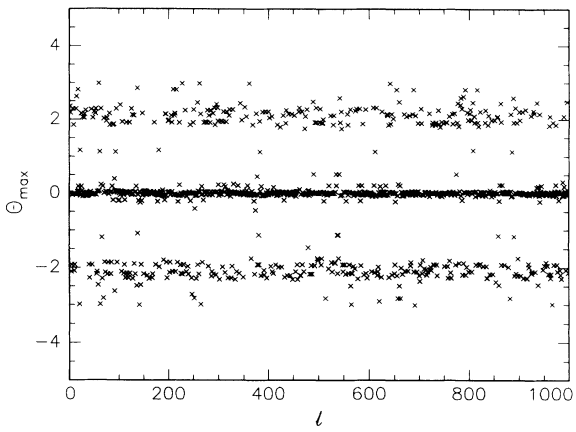

FIG. 2. The maximum in the probability density, θ_{max}, as a function of the iteration number l, for initial conditions which correspond to classical chaos. The persistence of peaks near $\theta_{max}=0$ and $\pm\theta_0$ is analogous to wave-function scarring. Although points lie near the classical-orbit points, they do not follow the classical sequence, so classical dynamics cannot be used to predict the most probable position of the particle.

The time-dependent scarring shown in Fig. 2 is associated with the same sixth-order periodic orbit described above. We consider the unstable case $\theta_0=2.05$, where the smallest deviation of the classical system from its periodic orbit will cause rapid wandering to distant regions of phase space. However, the corresponding quantum motion, as represented by the maximum in the probability density, appears remarkably faithful to this unstable classical orbit. The position of the maximum quantum probability density, θ_{max}, hovers about the unstable periodic points θ_0, 0, and $-\theta_0$. In Fig. 2 θ_{max} is displayed as a function of iteration number, l for $N=301$ and $\theta_0=2.05$.

Although the scar shown in Fig. 2 "remembers" the periodic orbit, one should not interpret time-dependent scarring as a quantum effect which allows wave functions to follow unstable classical motion. A careful examination of the points in Fig. 2 shows a crucial difference between the time dependence of θ_{max} and the (unstable) classical periodic motion. The points in Fig. 2 follow the classical sequence $(\theta_0,0,-\theta_0,-\theta_0,0,\theta_0)$ only for the first sixteen iterations ($l_c=17$). For $l \geq 17$, θ_{max} hops nearly randomly between points near θ_0, 0, and $-\theta_0$. The scar implies only the weakest remnant of classical motion, since classical predictability is lost.

B. Quantum echoes

Numerical investigations of the kicked Harper model reveal quantum echoes. An echo in the position of the centroid $\langle\theta\rangle$ at iteration $l \cong 450$ is shown in Fig. 3. This

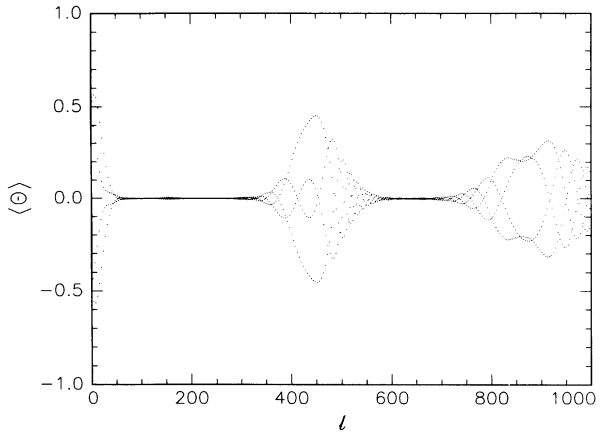

FIG. 3. An example of an echo in the motion of $\langle\theta\rangle$, plotted as a function of iteration number, with $\phi_0=0$, $\theta_0=\frac{1}{2}$, $g=\frac{3}{2}$, and $N=301$. The "echo" observed near $l\cong 450$ can be explained in terms of Bohr-Sommerfeld quantization of the orbit generated from iterations of the classical dynamics.

echo was obtained from the exact (except for numerical limitations) quantum dynamics using $\phi_0=0$, $\theta_0=\frac{1}{2}$, $g=\frac{3}{2}$, and $N=301$. The initial disperion of the wave packet (roughly linear in time) causes the initial damping of the oscillations in $\langle\theta\rangle$. The oscillations shown in Fig. 3 are accurately described by the semiclassical approximation, and the initial damping is accurately described by the first-order quantum correction. For this example, the semiclassical approximation with the first-order quantum correction fails for l greater than about 100. No sign of a quantum echo is seen in our formal expansion.

An intuitive explanation of the echo can be obtained by imposing the Bohr-Sommerfeld quantization condition on the phase-space orbit generated by the classical system

$$\oint \phi\, d\theta=(n+\gamma)(2\pi\hbar)\ ,$$

where n is an integer and γ is a small constant. Requiring a particle's coordinates to lie on one of these phase-space orbits gives a discrete separation between allowed values of the initial coordinates. For $\phi_0=0$, the allowed initial values of θ form a discrete set, $\theta(n)$. We have numerically followed the classical phase-space motion of this system for two initial conditions, one starting at $\theta(n)$ and the other starting at $\theta(n+1)$. These two initial points move about phase space with slightly different trajectories, so they slowly move apart from each other. Eventually, one point "catches" the other, and the two points again lie close to each other. For the initial conditions described in Fig. 3, we find that the number of iterations needed to produce this reconvergence of phase-space points ($l\cong 450$) coincides almost exactly with the time to the first echo shown in Fig. 3.

The echo illustrated in Fig. 3 corresponds to stable motion. We have observed weaker quantum echoes even when the corresponding classical motion is chaotic, but for this more complex case, where closed classical orbits do not exist, we have no simple explanation of the underlying physics.

VII. CONCLUSIONS

The kicked Harper model is particularly appealing because basic results can be obtained simply and physically. Stated briefly, our formal results are (1) the center of a wave packet obeys classical dynamics until the wave-packet dispersion becomes important; (2) chaos leads to exponential wave-packet explosion instead of ordinary wave-packet dispersion, and stable periodic orbits suppress the wave-packet dispersion; (3) corrections to the classical motion are given as a power series in $\hbar$, where the coefficients in the series are given by relatively simple recursion relations.

The Gaussian wave packets used to obtain these results provide physical insight. For example, the lowest-order spreading of these wave packets can be described in terms of classical motion and the Heisenberg uncertainty principle. This intuitive approach also shows how quantum corrections are related to distortions of the Gaussian wave packets.

Many of our results are closely related to those obtained for other systems. Our derivation of the correspondence between classical and quantum motion in the small-$\hbar$ limit is not a surprise. This is essentially Ehrenfest's theorem, and it has been derived for a variety of models in a variety of ways. Some results similar to ours have also been noted for wave-packet dispersion in the quantum version of the kicked rotor (Chirikov-Taylor map). Berry *et al.* [20] noted both slow and exponential rates of wave-packet spreading, and Berman and Zaslavsky [21] were apparently the first to associate the spreading rate with the classical stability. Fishman, Grempel, and Prange [6] used the classical correspondence to obtain scaling exponents for the wave-packet dispersion. Wave-packet delocalization was numerically traced by Skodje and Spina [22]. Fox and Lan [23] and Jensen and Niu [24] have generated power-series expansions in $\hbar$ which are similar in spirit to ours, although an exact correspondence is not clear. Work on the baker's map by O'Connor and Tomsovic [25] and by Ozorio de Almeida and Saraceno [26] showed the wave-packet spreading time is of order $\ln\hbar$ because the corresponding classical system is chaotic.

After the Gaussian wave packets disperse, our formal results based on wave-packet dynamics lose relevance. For longer times, we have used numerical simulations. We observed quantum echoes which could be explained in terms of a Bohr-Sommerfeld quantization condition for the regular phase-space orbits, and a time analog of scarring for chaotic motion. The Bohr-Sommerfeld quantization, and associated quantum echoes, suggest a uniform spacing of the quasienergy levels of the eigenstates of the time-evolution operator. The echo time is then essentially the inverse of the frequency interval separating these levels. On the other hand, the time-dependent scarring suggests a degree of localization of the eigenstates, but with nonuniform energy-level spacing. These results are not inconsistent with observations that regular motion leads to a nearly random distribution of energy levels because orbits with differing symmetries [27] or in differing regions of phase space can be random-

ly superposed and do not repel each other. The wave packets which exhibit quantum echoes are composed of a particular subset of eigenstates which have nearly uniform spacing.

There are many difficult problems associated with the relation between quantum mechanics and chaos which we have not addressed. In particular, it is not clear if chaos should be described only as an $\hbar \to 0$ limit for quantum systems, or if there is a purely quantum-mechanical characterization of systems which could be taken as "quantum chaos." For example, Fox [28] has described a spin in an electromagnetic field where the standard classical treatment (rotating wave) yields regular motion, but a semiclassical approach yields equations which can exhibit chaos. A rather artificial quantum system described by Chirikov *et al.* [29] is clearly chaotic. There have been a number of comments suggesting that additional insight could be obtained by examining the limits of large systems and long times, where the wave-packet picture does not apply. There have been studies [30–33] of possible chaos in infinite (open) systems, where discrete, absolutely continuous, and singular continuous spectra are clearly defined. Suggestions in these papers that the nature of the spectrum could be used to characterize quantum chaos are reasonable because one can relate the general characteristics of diffusion to the spectral properties of a system [34].

Finally, Ford, Manteca, and Ristow [35] have considered a quantum version of the map associated with the Arnol'd cat, and they claim a failure of the correspondence principle (in an appropriate limit). Does this mean that the $\hbar \to 0$ ($N \to \infty$) limit of the quantum kicked Harper model is in some sense different from the classical version of this system described by Eqs. (2)–(4a)? As Eckhardt notes [4], taking limits can be difficult, and we do not have an answer to this intriguing question.

*Permanent address: Physics Department, Indian Institute of Technology Kanpur, Kanpur, U.P. 208 016, India.

[1] M. Berry, Phys. Scr. **40**, 355 (1989).
[2] M. C. Gutzwiller, *Chaos in Classical and Quantum Mechanics* (Springer, New York, 1990).
[3] F. M. Izrailev, Phys. Rep. **196**, 229 (1990).
[4] B. Eckhardt, Phys. Rep. **163**, 205 (1988).
[5] G. Casati, B. V. Chirikov, F. M. Izrailev, and J. Ford, in *Stochastic Behavior in Classical and Quantum Hamiltonian Systems,* edited by G. Casati and J. Ford, Lecture Notes in Physics Vol. 93 (Springer, Berlin, 1979), p. 334.
[6] S. Fishman, D. R. Grempel, and R. E. Prange, Phys. Rev. Lett. **49**, 502 (1982).
[7] T. Geisel, G. Radons, and J. Rubner, Phys. Rev. Lett. **57**, 2883 (1986).
[8] E. Heller, Phys. Rev. Lett. **53**, 1515 (1984).
[9] O. Bohigas, M. J. Giannoni, and C. Schmidt, Phys. Rev. Lett. **52**, 1 (1984).
[10] G. M. Zaslavskii, M. Yu Zakharov, R. Z. Sagdeev, D. A. Usikov, and A. A. Chernikov, Pis'ma Zh. Eksp. Teor. Fiz. **44**, 349 (1986) [JETP Lett. **44**, 451 (1986)].
[11] G. Andre and S. Aubry, Ann. Isr. Phys. Soc. **3**, 133 (1980).
[12] J. B. Sokolov, Phys. Rep. **126**, 189 (1985).
[13] J. H. Lowenstein, Phys. Rev. A **43**, 4103 (1991).
[14] J. Lichtenberg and P. B. Wood, Phys. Rev. A **39**, 2153 (1989).
[15] V. V. Afanasiev, A. A. Chernikov, R. Z. Sagdeev, and G. M. Zaslavsky, Phys. Lett. A **144**, 229 (1990).
[16] P. Leboeuf, J. Kurchin, M. Feingold, and D. P. Arovas, Phys. Rev. Lett. **65**, 3076 (1990).
[17] D. Mei and D. P. Arovas (unpublished).
[18] T. Geisel, R. Ketzmerick, and G. Petschel, Phys. Rev. Lett. **67**, 3635 (1991).
[19] G. Casati, B. V. Chirikov, F. M. Izrailev, and J. Ford, in *Stochastic Behavior in Classical and Quantum Hamiltonian Systems,* edited by G. Casati and J. Ford, Lecture Notes in Physics Vol. 93 (Springer, Berlin, 1979), p. 334.
[20] M. V. Berry, N. L. Balazs, M. Tabor, and A. Voros, Ann. Phys. (N.Y.) **122**, 26 (1979).
[21] G. P. Berman and G. M. Zaslavsky, Dokl. Akad. Nauk SSSR **240**, 1082 (1978) [Sov. Phys.—Dokl. **23**, 410 (1978)].
[22] R. T. Skodje and A. Spina, Phys. Rev. A **42**, 6252 (1990).
[23] R. F. Fox and B. L. Lan, Phys. Rev. A **41**, 2592 (1990); B. L. Lan and R. F. Fox, *ibid.* **43**, 646 (1991).
[24] J. H. Jensen and Q. Niu, Phys. Rev. A **42**, 2513 (1990).
[25] P. W. O'Connor and S. Tomsovic, Ann. Phys. (N.Y.) **207**, 218 (1991).
[26] A. M. Ozorio de Almeida and M. Saraceno, Ann. Phys. (N.Y.) **210**, 1 (1991).
[27] J. C. Kimball and H. S. Dumas, Phys. Lett. A **144**, 201 (1990).
[28] R. J. Fox, Phys. Rev. A **44**, 6193 (1991).
[29] B. V. Chirikov *et al.*, Physica D **33**, 77 (1988).
[30] R. V. Mendes, J. Phys. A **24**, 4349 (1991).
[31] B. Dorizzi, B. Grammaticas, and Y. Pomeau, J. Stat. Phys. **37**, 93 (1984).
[32] St. Weigert, Z. Phys. B **80**, 3 (1990).
[33] B. Milek and P. Seba, Phys. Lett. A **151**, 289 (1985).
[34] J. C. Kimball, J. Phys. C **11**, 4347 (1978).
[35] J. Ford, G. Manteca, and G. H. Ristow, Physica D **50**, 493 (1991).